Title

Baseline Tumor Oxygen Saturation Correlates with a Pathologic Complete Response in Breast Cancer Patients Undergoing Neoadjuvant Chemotherapy

Journal

Cancer Research, 72(17)

ISSN

0008-5472

Authors

Ueda, Shigeto
Roblyer, Darren
Cerussi, Albert
et al.

Publication Date

2012-09-01

DOI

10.1158/0008-5472.can-12-0056

Clinical Studies

Cancer Research

Baseline Tumor Oxygen Saturation Correlates with a Pathologic Complete Response in Breast Cancer Patients Undergoing Neoadjuvant Chemotherapy

Shigeto Ueda[1,3], Darren Roblyer[1], Albert Cerussi[1], Amanda Durkin[1], Anais Leproux[1], Ylenia Santoro[1], Shanshan Xu[1], Thomas D. O'Sullivan[1], David Hsiang[2], Rita Mehta[2], John Butler[2], and Bruce J. Tromberg[1]

Abstract

Tissue hemoglobin oxygen saturation (i.e., oxygenation) is a functional imaging endpoint that can reveal variations in tissue hypoxia, which may be predictive of pathologic response in subjects undergoing neoadjuvant chemotherapy. In this study, we used diffuse optical spectroscopic imaging (DOSI) to measure concentrations of oxyhemoglobin (ctO_2Hb), deoxy-hemoglobin (ctHHb), total Hb ($ctTHb = ctO_2Hb + ctHHb$), and oxygen saturation ($stO_2 = ctO_2Hb/ctTHb$) in tumor and contralateral normal tissue from 41 patients with locally advanced primary breast cancer. Measurements were acquired before the start of neoadjuvant chemotherapy. Optically derived parameters were analyzed separately and in combination with clinical biomarkers to evaluate correlations with pathologic response. Discriminant analysis was conducted to determine the ability of optical and clinical biomarkers to classify subjects into response groups. Twelve (28.6%) of 42 tumors achieved pathologic complete response (pCR) and 30 (71.4%) were non-pCR. Tumor measurements in pCR subjects had higher stO_2 levels (median 77.8%) than those in non-pCR individuals (median 72.3%, $P = 0.01$). There were no significant differences in baseline ctO_2Hb, ctHHb, and ctTHb between response groups. An optimal tumor oxygenation threshold of $stO_2 = 76.7\%$ was determined for pCR versus non-pCR (sensitivity = 75.0%, specificity = 73.3%). Multivariate discriminant analysis combining estrogen receptor staining and stO_2 further improved the classification of pCR versus non-pCR (sensitivity = 100%, specificity = 85.7%). These results show that elevated baseline tumor stO_2 are correlated with a pCR. Noninvasive DOSI scans combined with histopathology subtyping may aid in stratification of individual patients with breast cancer before neoadjuvant chemotherapy. *Cancer Res; 72(17); 4318–28. ©2012 AACR.*

Introduction

Neoadjuvant chemotherapy has been recommended as a standard treatment for locally advanced breast cancer and is currently accepted for patients having operable breast cancer (1, 2). In the neoadjuvant setting, a pathologic complete response (pCR) is an important surrogate endpoint, as it is correlated with a favorable prognosis including longer disease-free survival and overall survival (OS; refs. 3–5). There is currently an effort to explore biomarkers associated with the mechanisms of chemosensitivity and response in breast cancer to aid in treatment planning and prognosis (6–8). Histologic markers used to determine tumor grade, proliferation, and biologic receptor status have been shown to be useful prognostic indicators (9). To date, there are no clinically accepted prognostic imaging endpoints available before treatment that can provide insight into the likelihood of an individual patient responding to neoadjuvant chemotherapy. Functional metrics that quantify tissue oxygen saturation, vascular supply and drainage, and tumor metabolism have been largely unexplored in this context and may be closely associated with chemosensitivity and therapy response.

Diffuse optical spectroscopic imaging (DOSI) is a noninvasive functional imaging modality that uses near infrared light to provide metabolic and hemodynamic information from thick tissues. DOSI is capable of measuring tissue concentrations (ct) of oxygenated hemoglobin (ctO_2Hb), deoxygenated hemoglobin (ctHHb), water (ctH_2O), and lipid (10). These measurements are directly related to tumor metabolism and vascular characteristics. For example, high levels of tumor ctO_2Hb are considered to be a surrogate marker for elevated vascular supply potentially due to angiogenesis. High levels of ctHHb reflect high oxygen consumption and tissue metabolism due to tumor proliferation and/or poor vascular drainage. Total hemoglobin concentration (ctTHb) corresponds to

Authors' Affiliations: [1]Laser Microbeam and Medical Program (LAMMP), Beckman Laser Institute and Medical Clinic, University of California, Irvine; [2]Chao Family Comprehensive Cancer Center, University of California, Irvine Medical Center, Orange, California; and [3]Department of Breast Oncology, Saitama International Medical Center, Saitama Medical University, Saitama, Japan

Note: S. Ueda and D. Roblyer contributed equally to this work.

Corresponding Author: Bruce J. Tromberg, Beckman Laser Institute and Medical Clinic, University of California, Irvine, 1002 Health Sciences Road, Irvine, CA 92612. Phone: 949-824-8705; Fax: 949-824-8413; E-mail: bjtrombe@uci.edu

doi: 10.1158/0008-5472.CAN-12-0056

the total blood volume in tumors and has been validated as an index that corresponds to increased vascular density (11). Low oxygen saturation [stO_2, defined as $ctO_2Hb/(ctO_2Hb + ctHHb)$] is an indication of tumor hypoxia or necrosis. Several investigators have reported a relationship between hypoxic tumors and lower partial pressure of oxygen (pO_2; refs. 12–14), and stO_2 has been shown as a surrogate of pO_2 by several studies conducted using erythrocyte-containing phantoms (15–17).

Previous studies by our group and others have shown that DOSI and similar techniques are able to localize and characterize functional properties of breast tumors at baseline (18) and during neoadjuvant treatment (19–22). Significant changes in hemoglobin, water, and lipid over the first weeks of therapy have been shown to correlate with overall pathologic response. All these studies examined the impact of neoadjuvant chemotherapy on tumor physiology in individual patients over the course of lengthy regimens.

In this research, we investigate, for the first time, the relationship between baseline tumor properties determined by DOSI and final post-surgical pathologic response. We hypothesize that DOSI functional measurements before surgery can provide information that correlates with clinical outcome. This is due to the direct relevance of DOSI-measured properties on tumor perfusion and metabolism, which, in turn, impact the delivery and use of chemotherapeutic drugs. Similar attempts have been made to predict neoadjuvant therapy response based on imaging endpoints obtained before treatment using MRI (23, 24), diffusion-weighted MRI (DW-MRI; refs. 25, 26), and molecular imaging techniques, [e.g. positron emission tomography (PET); refs. 27, 28]. These studies were designed to assess either pretreatment anatomic features of tumors (MRI), the diffusion of water in tumor tissue (DW-MRI), or the uptake of glucose and magnitude of blood flow (^{18}FDG-PET and ^{15}O-water). Because DOSI parameters reveal intrinsic physiologic properties of tumors such as metabolism and perfusion, they may be broadly applicable to different chemotherapeutic strategies and have the added advantage of not requiring exogenous contrast agents.

This retrospective study examines 41 primary patients with breast cancer who received neoadjuvant chemotherapy and enrolled in a University of California, Irvine (Irvine, CA) Institutional Review Board optical imaging clinical protocol over a period of 7 years. Baseline DOSI measurements show that pretherapy tumor tissue oxygen saturation, stO_2, (also known as oxygenation) is the single best DOSI-derived predictor of pCR. In addition, we show that DOSI imaging endpoints can enhance the use of conventional biomarkers, such as hormone receptor status, potentially providing new insight for treatment planning and optimization before initiating therapy.

Patients and Methods

DOSI instrumentation

Details of the instrumentation are provided elsewhere (10). Briefly, DOSI uses near infrared light (650–1,000 nm) from 6 laser diodes and a broadband lamp to determine the optical scattering and absorption properties of thick tissue such as the breast. Laser diode output is amplitude modulated between 50 and 600 MHz. Amplitude and phase delay of detected signals are used as inputs into an analytic model of diffuse light transport to determine tissue scattering and absorption coefficients at the laser wavelengths. A broadband lamp is also used to illuminate tissue and the detected reflectance spectrum is scaled so that absorption is determined continuously over the entire spectral range. Absolute tissue concentrations of $ctHbO_2$, ctHHb, ctH_2O, and lipid are calculated by fitting known absorption spectra from these quantities to the measured absorption spectrum. ctTHb is defined as $ctHbO_2 + ctHHb$, and stO_2 is $ctHbO_2/(ctHbO_2 + ctHHb)$.

A handheld probe is used to acquire measurements in patients. The probe houses illumination optical fibers that transport light from the laser diodes and broadband lamp, an avalanche photodiode detector (APD) that detects laser light, as well as the distal end of an optical fiber that transports broadband light to a spectrometer. Measurements are conducted by placing the handheld probe on the tissue with light pressure so that there is adequate optical contact. We have shown in previous studies that this procedure does not require compression, does not influence tissue optical property measurements, and optical contrast is available even from small (<15 mm) tumors embedded millimeters or centimeters below the surface of the skin (18, 29).

Patient measurements

This is a retrospective analysis of 41 patients with newly diagnosed, operative, and primary breast cancer measured between October 2004 and March 2010. All patients provided informed consent and participated in this study under a clinical study approved by institutional review committee of the University of California, Irvine. Women were excluded if they were pregnant or were younger than 21 years or older than 75 years. Subjects were included in this analysis if they (i) received neoadjuvant chemotherapy before surgical resection of tumors, (ii) were measured with the DOSI system at least 14 days after core biopsy and before neoadjuvant chemotherapy treatment (average, 31.3 days; 14–110), and (iii) had evaluable DOSI measurements. Of the 48 subjects measured during the study period, 6 subjects were determined to be nonevaluable. Nonevaluable measurements include measurements in which a laser diode was malfunctioning ($n = 3$), a subject had an implant in close proximity to the tumor ($n = 1$), or when the tumor was retro-areolar and it was not possible to distinguish contrast from tumor and contrast from areola ($n = 2$). One additional subject was excluded because of a diagnosis of inflammatory breast cancer. All subjects included in the study were histologically diagnosed with invasive ductal or lobular carcinoma before neoadjuvant treatment. Age, tumor location, tumor size, clinical stage, and histologic grading were obtained from patients' medical records. Estrogen receptor (ER), progesterone receptor (PR), Ki67 staining, and c-erbB2 (HER2) were immunohistochemically assessed in the specimens obtained by core biopsy.

Patients were measured in a supine position using a handheld probe placed against the breast tissue. Sequential measurements were taken in a rectangular grid pattern marked on

the breast with each point separated by 10 mm. Measurements were taken to include the area of the underlying tumor as determined by ultrasound and palpation, as well as a margin of surrounding normal tissue. Contralateral normal breast measurements were collected from patients with unilateral breast cancer. A point measurement was acquired in fewer than 30 seconds and total measurement time varied between 20 minutes and 1 hour per patient. A detailed video description of the patient measurement procedure developed for an ongoing American College of Radiology Imaging Networks (ACRIN) clinical trial (ACRIN 6691) is available (30).

Mean values of tumor ctO_2Hb, ctHHb, ctTHb, and stO_2 were calculated by averaging DOSI measurements taken on breast tissue corresponding to regions of interest (ROI) using a previously described method (31). Briefly, ROIs were determined by palpation, mammography, ultrasound, and MRI (if available) to contain tumor. Tumor locations were additionally confirmed by an increase in ctHHb and water and a decrease in lipids measured with DOSI. This combination of chromophore values, designated as the tissue optical index (TOI), has been previously shown to be a consistent indicator of tumor location (32). Optical parameters from contralateral normal breast tissue were also measured in corresponding mirror image locations. The measurement procedure and example optical property maps are shown in Fig. 1.

For the relatively large tumors measured in this study (mean, 3.5 cm in largest dimension), ROIs included at least 3 and typically 5 discrete measurement points. Each optical parameter value reported is therefore a mean of the approximately 5 values within the ROI, and the SD is a reflection of the physiologic variation for that patient. This contrasts with the intrinsic instrument precision (relative SD), which has been well-characterized on the basis of repetitive measurements of homogeneous tissue phantoms and human breast tissue to less than 5% for all relevant parameters (29).

Neoadjuvant chemotherapy regimen

Twenty-four (58.5%) of 41 patients received a chemotherapy regimen that consisted of doxorubicin (60 mg/m^2) intravenously and cyclophosphamide (AC regimen; 600mg/m^2) intravenously every 14 days for 2 to 4 cycles with pegfilgrastim support, depending on clinical response. This treatment was followed sequentially with paclitaxel or nab-particle paclitaxel (100 mg/m^2), as well as weekly carboplatin [area under the curve (AUC) = 2] for 3 weeks followed by 1 week of rest, for 9 to 12 doses. Concurrent trastuzumab therapy was administered at 4 mg/kg loading dose, followed by a maintenance dose of 2 mg/kg weekly for 10 to 12 cycles in 4 patients with HER2-positive tumor. Concurrent bevacizumab therapy was administered at 10 mg/kg every 2 weeks for 5 to 6 doses in 11 patients.

Seventeen (41.5%) patients received a concurrent regimen of carboplatin and nab-paclitaxel combined with trastuzumab for 10 to 12 cycles or with bevacizumab for 10 to 12 cycles, respectively. This was sequentially followed by AC regimens depending on clinical response.

Histological grading system

The histologic grading system was based on 3 morphologic features consisting of nuclear pleomorphism of tumor cells, degree of tumor tubule formation, and mitotic activity (33). Scores of all 3 components are added together to give the grade,

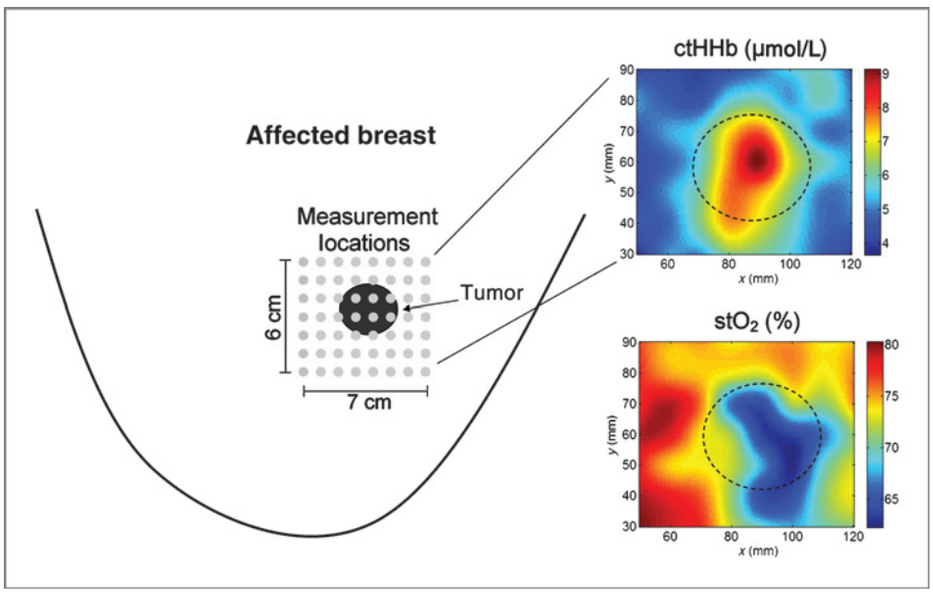

Figure 1. DOSI measurement procedure and optical property maps. Measurements are taken using a handheld probe that is moved in a grid or line pattern over tumor and normal breast tissue. Dots indicate measurement locations. In this example, an 6 cm by 7 cm region of tissue was measured containing a clinical stage II IDC measured to be 27 mm in the greatest dimension. Maps of optical properties are made by interpolating data values between measurement points. In this example, both deoxyhemoglobin (ctHHb) and oxygen saturation (stO_2) are shown. In both maps, which are from identical tissue locations, the dotted circle indicates the approximate tumor location determined by ultrasound and palpation. This subject was non-pCR. Note the relatively low oxygen saturation in the tumor region compared with surrounding normal tissue.

score 3 to 7. Grade was classified into low-grade (III–V) and high-grade (VI–IX).

Immunohistochemistry

Formalin-fixed, paraffin-embedded tissues obtained for diagnostic core biopsy were used for this study. Immunohistochemistry was conducted on 5-μm thick tissue sections. After deparaffination and rehydration, endogenous peroxidase activity was blocked for 10 minutes in a methanol solution that contained 0.3% hydrogen peroxidase. After antigen retrieval with 10-minute microwave in 10 mmol/L sodium citrate (pH 6.0), a cooling-off period of 20 minutes preceded the incubation of the primary antibodies. Briefly, ER antibody (1D5, Dako), PR antibody (PgR636, Dako), and Ki67 (MIB1, Dako) were ready-to-use agents with overnight incubation in a cold room. All antibodies were detected with the standard streptavidin–biotin complex method with 3,3′-diaminobenzidine as the chromogen. All stainings were developed with anti-polyvalent, HRP/DAB detection system and counterstained for 15 minutes with hematoxylin and eosin. HER2 testing was done according to the protocol of Herceptest Kit (Dako). Breast cancer tissues previously determined to have positive results were used as positive controls.

Evaluation of immunohistochemical biomarkers

Percentage of ER and PR immunostaining was calculated on the basis of the fraction of positive tumor cells to whole tumor cells (<5% of nuclei staining, negative; 5%–100% of nuclei staining, positive). For Ki67, the index was estimated by counting the percentage of Ki67-positive cell nuclei per a minimum of 400 cancer cells in areas with the highest mitotic activity at low-power fields (×40) in representative sections of the tumors. HER2 status was determined by immunohistochemistry or FISH analysis. Tumors with a score 3+ (entire circumference of the cell membrane was strongly stained) or tumors that amplified Her2/neu gene by FISH were defined as positive.

Pathological response

All specimens excised from the breast were sectioned into 5-μm-thick slices and were microscopically analyzed for the presence of residual tumor by a board certified pathologist. pCR was defined as microscopic evidence that invasive components of cancer cells had entirely disappeared in all inspected pathologic specimens. Regional lymph node involvement was not evaluated in this study. The tumors that did not achieve pCR were considered to be non-pCR.

Surgery

Surgery was planned 3 to 5 weeks after the final course of chemotherapy was delivered. Conservative surgery with lumpectomy or segmentectomy was chosen depending on tumor size and its location after tumor shrinkage. In patients who achieved a significant response to chemotherapy, an ultrasonographic examination was conducted before surgery to assist in confirming the location of the lesion. The remaining patients underwent a modified radical mastectomy. In all patients, axillary dissection was conducted.

Statistical analysis

Statistical comparisons between response groups were computed using JMP software (Cary). Unpaired 2-sided Student *t* tests and the Wilcoxon test were used to compare differences in tumor values (T), contralateral normal values (N), and normalized (T-N) values of ctO_2Hb, ctHHb, ctTHb, stO_2 as well as ER staining, PR staining, Ki67 staining, and tumor size between pCR and non-pCR groups. Fisher exact test was used to compare HER2 status and grade between response groups. P values <0.05 were considered significant.

Discriminant analysis was conducted using MATLAB (MathWorks). Two classification algorithms were used, a linear classifier based on Bayesian parameter estimation, which assumed multivariate normal densities and equal covariances for each group, and a ordinal logistic regression model, which does not assume the data are normally distributed. *A priori* probabilities for the linear discriminant classifier were based on the relative proportion of each group. Five-fold cross-validation was used for all classifiers to mitigate potential overperformance in this relatively small data set. Receiver-operating characteristic (ROC) curves were constructed using computed posterior probabilities calculated from the classifiers. The AUC of the ROC curve was used as an overall performance metric for the classifier. Sensitivity, specificity, negative predictive values, and positive predictive values were also reported at the optimal threshold or *Q*-point. The *Q*-point is the operating point on the ROC curve that has the minimum geometric distance from the upper left hand corner of the plot. For multivariate discrimination analysis, AUCs were compared from classifiers using all possible combinations (2 at a time) of the following features: ctO_2Hb, ctHHb, ctTHb, stO_2, ER staining, PR staining, Ki67 staining, and tumor size.

A 1-way ANOVA was conducted to estimate the inter- and intratumor variance for each optical parameter, and the F test was applied to test the null hypothesis of no difference between these variances.

Results

Baseline characteristics of tumors

Forty-one patients were measured in this study. One patient had bilateral disease so a total of 42 tumors were evaluated for this study. There was at least a 14-day interval (average, 31.3 days; 14–110) between the diagnostic core biopsy and the baseline DOSI measurements before the beginning of neoadjuvant chemotherapy. The average number of days between the baseline DOSI measurement and the first infusion was 11.7 ± 10.7 days. Table 1 displays subject and tumor characteristics. Twelve (28.6%) tumors achieved pCR and 30 (71.4%) tumors were defined as non-pCR. pCR rate did not differ between subjects who received chemotherapy alone and those who received monoclonal antibody combination regimens ($P = 0.4$; Student t test).

Comparison of optical properties and biomarkers in subjects achieving pCR and non-pCR

Table 2 shows the mean and median of tumor, normal, and tumor-normal (T-N) values of ctO_2Hb, ctHHb, ctTHb, stO_2, as

Table 1. Patient and tumor characteristics

Variables	Totals ($N = 42$) *n* (%)
Age, y	
Mean ± SD	49.2 ± 11.2
Tumor size, cm	
Mean ± SD	3.5 ± 2.1
Menopause	
Pre	23 (54.8)
Post	19 (45.2)
Location	
Left	21 (50)
Right	21 (50)
Histology	
IDC	36 (85.7)
ILC	5 (11.9)
IDC + ILC	1 (2.4)
Histologic grade	
Score 3–6	14 (33.3)
Score 7–9	25 (59.5)
Unknown	3 (7.1)
T stage	
I	7 (16.7)
II	25 (59.5)
III	7 (16.7)
IV	3 (7.1)
Nodal status	
−	8 (19)
+	34 (81)
ER status (cutoff 5%)	
−	12 (28.6)
+	28 (66.7)
Unknown	2 (5)
PR status (cutoff 5%)	
−	14 (33.3)
+	26 (61.9)
Unknown	2 (5)
HER2 status	
0, 1+, 2+ (FISH−)	29 (69)
3+ or FISH+	10 (23.8)
Unknown	3 (7.1)
Chemotherapy regimen	
Chemotherapy alone	13 (31)
Trastuzumab combo	9 (21.4)
Bevacizumab combo	20 (47.6)
Surgical procedure	
Mastectomy	29 (69)
Segmentectomy	4 (9.5)
Lumpectomy	9 (21.4)
Pathologic response	
Non-pCR	30 (71.4)
pCR	12 (28.6)

NOTE: Monoclonal antibody combinations include trastuzumab or bevacizumab with chemotherapy.
Abbreviations: IDC, invasive ductal carcinoma; ILC, invasive lobular carcinoma.

well as tumor size, ER staining, PR staining, Ki67 staining, tumor grade, and HER2 status for both the pCR and non-pCR groups. The stO_2-T measured in subjects achieving pCR was higher than non-pCR (median, 77.8% vs. 72.3%; $P = 0.02$, Student t test; $P = 0.01$, Wilcoxon). There were no significant differences between response groups for the optical parameters ctO_2Hb-T ($P = 0.4$, Student t test; $P = 0.3$, Wilcoxon), ctHHb ($P = 0.2$, Student t test; $P = 0.3$, Wilcoxon), and ctTHb ($P = 0.7$, Student t test; $P = 0.5$, Wilcoxon).

There were significant differences between response groups in ER ($P < 0.0001$, Student t test; $P < 0.0001$, Wilcoxon), PR ($P = 0.01$, Student t test; $P = 0.002$, Wilcoxon), Ki67 ($P = 0.005$, Student t test; $P = 0.02$, Wilcoxon), and HER2 status ($P = 0.04$, Fisher exact test). Tumor size and grade were not significantly different between response groups ($P = 0.3$, Student t test; $P = 0.1$, Wilcoxon for tumor size; $P = 0.2$, Fisher exact test for tumor grade).

Figure 2 shows box-and-whisker plots of stO_2 levels in pCR and non-pCR in both tumor and contralateral normal tissue. As described above, stO_2-T measurements were significantly higher in tumor tissue measured in subjects achieving pCR than non-pCR ($P = 0.02$, Student t test; $P = 0.01$, Wilcoxon). The stO_2 measurements from contralateral normal tissue did not show significant differences between pCR and non-pCR response groups (median, 77.4% vs. 77.5%; $P = 0.97$, Student t test; $P = 0.98$, Wilcoxon). When stO_2 measured in normal tissue was subtracted from stO_2 measured in paired tumor tissue (stO_2-T-N), no statistical differences were detected between pCR and non-pCR groups (median, 0.3% vs. −3.22%; $P = 0.06$, Student t test; $P = 0.05$, Wilcoxon).

The stO_2-T levels in pCR and non-pCR tumors were stratified by either chemotherapy alone, trastuzumab combined with chemotherapy, or bevacizumab combined with chemotherapy. There were significant differences between tumor stO_2 in the pCR and non-pCR groups when chemotherapy was used alone using t tests but not with the Wilcoxon test (median, 80.5% vs. 76.1%, $P = 0.05$, Student t test; $P = 0.06$, Wilcoxon). Although not significant, the same trend occurred when chemotherapy was combined with trastuzumab (median, 77.4% vs. 71.7%; $P = 0.2$, Student t test; $P = 0.3$, Wilcoxon). There was an insufficient number of tumors treated with bevacizumab that achieved pCR ($n = 3$) to statistically compare stO_2 values in this treatment subgroup.

It is of note that the mean intratumor variation was significantly lower than the intertumor variation for stO_2, ctO_2Hb, ctHHb, ctTHb, and TOI. Model-based estimates of the inter- and intratumor SDs and the P values for the F test with 41 and 186 degrees of freedom are as follows: stO_2 (16.4, 3.2, $P < 0.0001$), ctO2Hb (20.5, 7.4, $P < 00001$), ctHHb (6.7, 1.4, $P < 0.0001$), ctTHb (24.9, 7.8, $P < 0.0001$), and TOI (7.8, 2.6, $P < 0.0001$).

Discriminant analysis

Performance of the linear discriminant classifier and the ordinal logistic classifier were compared and the AUC values for both classifiers are shown in Table 3. Because the difference between the models did not change the outcome or our conclusions, thresholds, sensitivity, specificity, positive

Table 2. Baseline optical and tissue biomarker values for tumors achieving pCR and non-pCR

		pCR			Non-pCR		Student *t* test	Wilcoxon test
Variables	***N***	**Mean (95% CI)**	**Median**	***N***	**Mean (95% CI)**	**Median**	***P***	***P***
A. Continuous parameter								
ctO_2Hb-T, μmol/L	12	26.1 (20.4–31.7)	24.7	30	23.4 (19.8–26.9)	20.7	0.4	0.3
ctHHb-T, μmol/L	12	7.32 (5.39–9.24)	6.67	30	8.64 (7.42–9.85)	7.64	0.2	0.3
ctTHb-T, μmol/L	12	33.4 (26.3–40.4)	31.3	30	32.0 (27.6–36.5)	28.9	0.7	0.5
stO_2 (%)-T	12	77.8 (74.0–81.5)	77.8	30	72.3 (69.9–74.7)	73.8	0.02[a]	0.01[a]
TOI-T	12	4.75 (2.38–7.12)	3.18	30	5.47 (3.97–6.97)	4.29	0.6	.5
ctO_2Hb-N, μmol/L	11	15.2 (12.1–18.3]	14.8	22	16.5 (14.2–18.7)	15.4	0.5	0.6
ctHHb-N, μmol/L	11	4.22 (3.24–5.20)	4.22	22	4.7 (3.99–5.38)	4.15	0.4	0.8
ctTHb-N, μmol/L	11	19.4 (15.7–23.2)	18.8	22	21.1 (18.5–23.8)	19.6	0.5	0.5
stO_2-N, %	11	77.4 (74.1–80.8)	77.7	22	77.5 (75.2–79.9)	78.1	0.97	0.98
TOI-N	11	1.14 (0.39–1.88)	0.91	22	1.66 (1.14–2.19)	1.17	0.3	0.6
ctO_2Hb-T-N, μmol/L	11	10.0 (4.21–15.8)	8.67	22	7.59 (3.48–11.7)	5.35	0.5	0.2
ctHHb-T-N, μmol/L	11	2.70 (0.67–4.74)	2.13	22	3.65 (2.21–5.09)	2.29	0.4	0.98
ctTHb-T-N, μmol/L	11	12.7 (5.36–20.1)	10.7	22	11.2 (6.03–16.45)	8.12	0.7	0.4
stO_2-T-N, %	11	0.56 (−3.24 to 4.36)	0.30	22	−3.97 (−6.66 to −1.29)	−3.22	0.06	0.05
TOI-T-N	11	2.75 (0.74–4.76)	1.67	22	3.24 (1.82–4.66)	2.37	0.7	0.8
Tumor size, cm	12	2.89 (1.66–4.12)	2.40	30	3.70 (2.92–4.48)	2.95	0.3	0.1
ER (%)	12	18.3 (0.02–36.5)	0.00	28	83.5 (71.6–95.4)	95.0	<0.0001[a]	<0.0001[a]
PR (%)	12	16.3 (−7.56 to 40.1)	0.00	28	53.2 (37.6–68.8)	70.0	0.01[a]	0.002[a]
Ki67 (%)	9	58.0 (41.5–74.5)	60.0	21	28.5 (17.7–39.3)	20.0	0.005[a]	0.02[a]

B. Binary parameter			
Variables	**pCR**	**Non-pCR**	**Fisher exact test (*P*)**
Grade			
High	10	15	
Low	2	12	0.2
Unknown	0	3	
HER2 status			
Positive	6	4	
Negative	6	23	0.04[a]
Unknown	0	3	

NOTE: For continuous variables, *P* values from both the Student *t* test and Wilcoxon test are shown. For binary variables, *P* values from Fisher exact test are shown.

Abbreviation: CI, confidence interval.

[a]Statistically significant result.

predictive values, and negative predictive values are only shown for the linear discriminant classifier.

Table 3 shows classification results from optically derived parameters (ctO_2Hb, ctHHb, ctTHb, stO_2 from tumor site, normal site, and tumor-normal) and clinical biomarkers (ER, PR, Ki67, and tumor size). ER staining was the best performing parameter with an AUC of 0.854, sensitivity of 91.7%, specificity of 82.1%, positive predictive value of 68.8%, and negative predictive value of 95.8%. The optimal threshold for ER staining was 79.6%, although it is of note that similar performance could be achieved over a wide range of threshold values as subjects generally had none, very low staining (<10%), or very high staining (>85%). The stO_2-T was the best performing optically derived parameter and the second best parameter overall with an AUC of 0.733, sensitivity of 75.0%, specificity of 73.3%, positive predictive value of 52.9%, and negative predictive value of 88.0%. The optimal threshold for stO_2 was 76.7%. The normalized tumor value, stO_2 (T-N), was the second best performing optically derived parameter and the fourth best parameter overall with an AUC of 0.692, sensitivity of 81.8%, specificity of 59.1%, positive predictive value of 50.0%, and negative predictive value of 86.7%.

The best performing combination of 2 parameters in the multivariate discriminant analysis was ER staining and stO_2-T (see Fig. 3). When these parameters were used together to discriminate response groups, an AUC of 0.955 was achieved

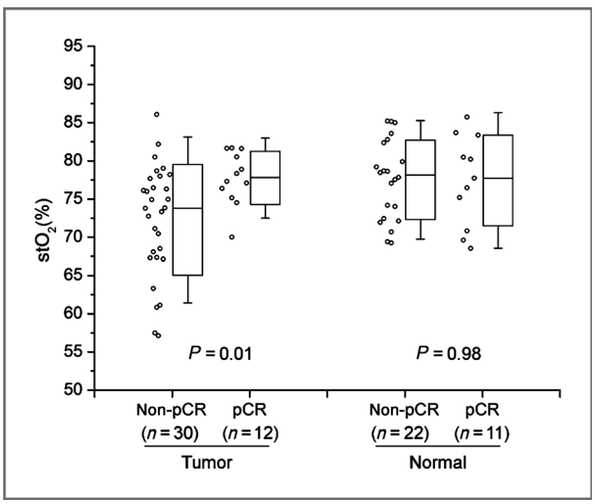

Figure 2. Box-and-whisker plots showing the difference in tumor stO_2 levels between pCR and non-pCR tumors (left; median, 77.8% vs. 72.3%; $P = 0.01$, Wilcoxon) and the lack of difference in stO_2 levels between contralateral normal tissues (middle; median, 77.7% vs. 78.1%; $P = 0.98$, Wilcoxon).

with a sensitivity of 100%, specificity of 85.7%, positive predictive value of 75.0%, and negative predictive value of 100%. This combination provides an 11.8% increase in AUC over using ER staining alone and a 30.3% increase over stO_2-T alone. Table 3 also shows the highest performing combinations of optical and clinical biomarkers for each biomarker. Other combinations that achieved a high classification accuracy included ER and BRS grade (AUC, 0.897), ER and ctHHb (AUC, 0.871), and ER and ctO_2Hb (AUC, 0.859).

Statistical significance between ROC curves was determined using the methods described in the work of Vergara and colleagues (34). Posterior probabilities output from the discriminant analysis for the predictors of ctO_2Hb, ctHHb, ctTHb, stO_2, ER, PR, tumor size, stO_2 + ER, stO_2 + PR, and stO_2 + tumor size were used as inputs for the comparison. The method requires sample sizes for each predictor to be equivalent and 2 data points were removed from several of the predictors to meet this criterion. Ki67 was not compared with the other predictors, as only 30 samples were available. The combination of stO_2 + ER was statistically different ($P < 0.05$) from all other predictors except for ER ($P = 0.23$) implying that this combination provides information not available from the other predictors.

Discussion

In this retrospective analysis of 41 patients measured over a period of 7 years using a standardized optical imaging technology, we observed that patients who exhibited a pCR to neoadjuvant chemotherapy had higher tumor tissue hemoglobin oxygen saturation (stO_2) values than non-pCR subjects. In addition, tumor stO_2 levels measured in subjects achieving pCR were similar or higher than levels measured in paired normal tissue. In contrast, non-pCR tumors had lower stO_2 than in normal tissue. Finally, stO_2 levels were not different between response groups in contralateral normal breast tissue. These findings support the idea that pCR and non-pCR tumors have differential oxygen delivery and use. These results highlight the potential use of DOSI measurements for understanding *in vivo* tumor biology and represent one of the first applications of functional imaging for chemotherapy response prediction using baseline measurements alone.

Discriminant analyses revealed the significance of tumor stO_2 as a prognostic indicator of chemotherapy responsiveness. ROC analysis showed that tumor stO_2 alone was sufficient to separate pCR from non-pCR response groups (AUC, 0.733) with comparable accuracy to established predictive markers such as ER (AUC, 0.854), PR (AUC, 0.707), Ki67 (AUC, 0.672), and tumor size (AUC, 0.607). A sensitivity of 75.0% and specificity of 73.3% was shown for the classification of pCR using an optimal stO_2 threshold of 76.7%.

We also explored the prognostic capability of more traditional biomarkers to predict pCR alone and in combination with optical markers. In confirmation of well-established trends, we observed that lower hormone receptor expression and higher proliferation as measured by Ki67 were both correlated with pCR (35–37). Furthermore, when stO_2 and ER were used together in a multivariate discriminant analysis, classification of response groups improved (AUC, 0.955). The combination of stO_2 and ER was the best pairing of the measured parameters. This finding suggests that the noninvasive optical measurements explored in this study provide independent prognostic information that may be able to supplement current standard of care tissue molecular biomarkers. It should be noted that only 2 parameters were tested at a time for the discriminant analysis due to a relatively small sample size. This did not allow for control of multiple other covariates simultaneously. It is also of note that the predictive value of ER alone in this study was excellent (sensitivity: 92%, specificity: 82%) and other studies have reported more modest correlations with response. For example, in 3 separate studies of more than 200 subjects receiving neoadjuvant chemotherapy for breast cancer with chemotherapy regimens similar to those in this study, the predictive value of ER negativity was sensitivity of 88%, specificity of 50%; sensitivity of 64%, specificity of 63%; and sensitivity of 90%, specificity of 61% (35, 38, 39). The discrepancy is likely due to the small sample size in this study.

In contrast to our previous work in which we showed a correlation between normalized baseline oxyhemoglobin concentration and neoadjuvant chemotherapy response in a small cohort of patients ($n = 11$) all receiving the same drug regimen (19), this study shows that non-normalized stO_2 measurements are of prognostic significance in a much larger group of patients ($n = 41$) receiving various chemotherapy regimens. Absolute measurements are advantageous, because they do not rely on a choice of a normal tissue site and could potentially be implemented into clinical practice as a tumor measurement with a clearly defined saturation threshold (76.7%). Furthermore, we have shown here that combining optical endpoints with clinical biomarkers significantly improves discrimination between responders and nonresponders.

Table 3. Predictive performance of optical and tissue biomarkers using univariate and multivariate discriminant analyses

Parameter	*n*	Threshold	AUC (logistic)	AUC (LDA)	Sensitivity	Specificity	PPV	NPV
Optical properties								
stO_2-T	42	76.7%	0.733	0.719	75.0% (42.8%–93.3%)	73.3% (53.8%–87.0%)	52.9% (28.5%–76.1%)	88.0% (67.7%–96.8%)
$ctHbO_2$-T	42	25.4 μmol/L	0.506	0.536	40.0% (22.3%–77.7%)	66.7% (47.1%–82.1%)	37.5% (16.3–64.1%)	76.9% (55.9%–90.2%)
ctHHb-T	42	7.51 μmol/L	0.576	0.599	66.7% (35.4%–88.7%)	53.3% (34.6%–71.2%)	36.4% (18.0%–59.2%)	80.0% (55.7%–93.4%)
ctTHb-T	42	33.4 μmol/L	0.419	0.506	50.0% (22.3%–77.7%)	53.3% (34.6%–71.2%)	30.0% (12.8%–54.3%)	72.7% (49.6%–88.4%)
stO_2-T-N	33	−2.51%	0.692	0.669	81.8% (47.8%–96.8%)	59.1% (36.7%–78.5%)	50.0% (26.8–73.2%)	86.7% (58.4%–97.7%)
$ctHbO_2$-T-N	33	8.40 μmol/L	0.545	0.502	45.5% (18.1%–75.4%)	77.3% (54.2%–91.3%)	50.0% (20.1%–79.9%)	73.9% (51.3%–88.9%)
ctHHb-T-N	33	2.46 μmol/L	0.471	0.450	72.7% (39.3%–92.7%)	50.0% (28.8%–71.2%)	42.1% (21.1%–66.0%)	78.6% (48.8%–94.3%)
ctTHb-T-N	33	10.9 μmol/L	0.488	0.396	36.4% (12.4%–68.4%)	77.3% (54.2%–91.3%)	44.4% (15.3%–77.3%)	70.8% (48.8%–86.6%)
Biomarkers								
ER	40	79.6%	0.854	0.860	91.7% (59.8%–99.6%)	82.1% (62.4%–93.2%)	68.8% (41.5%–87.9%)	95.8% (76.9%–99.8%)
PR	40	7.61%	0.707	0.705	83.3% (50.9%–97.1%)	67.9% (47.6%–83.4%)	52.6% (29.5%–47.8%)	90.5% (68.2%–98.3%)
Ki67	30	48.2%	0.672	0.685	66.7% (30.9%–91.0%)	76.2% (52.4%–90.9%)	54.5% (24.6%–81.9%)	84.2% (59.5%–95.8%)
Tumor size	42	2.64 cm	0.607	0.661	75.0% (42.8%–93.3%)	63.3% (43.9%–79.5%)	45.0% (23.8%–68.0%)	86.4% (64.0%–96.4%)
Combination								
stO_2-T + ER	40	NA	0.955	0.933	100% (69.9%–100%)	85.7% (66.4%–95.3%)	75.0% (47.4%–91.7%)	100% (82.8%–100%)
stO_2-T + PR	40	NA	0.813	0.802	75.0% (42.8%–93.3%)	78.6% (58.5%–91.0%)	60.0% (32.9%–82.5%)	88.0% (67.7%–96.8%)
ctHHb-T + Ki67	30	NA	0.773	0.735	77.8% (40.2%–96.1%)	81.0% (57.4%–93.7%)	63.6% (31.6%–87.6%)	89.5% (65.5%–98.2%)
stO_2-T + tumor size	42	NA	0.681	0.696	66.7% (35.4%–88.7%)	66.7% (47.1%–82.1%)	44.4% (22.4%–68.7%)	83.3% (61.8%–94.5%)
stO_2-T-N + ER	32	NA	0.896	0.890	90.9% (57.1%–99.5%)	90.5% (68.2%–98.3%)	83.3% (50.9%–97.1%)	95.0% (73.1%–99.7%)
stO_2-T-N + PR	32	NA	0.706	0.710	63.6% (31.6%–87.6%)	81.0% (57.4%–93.7%)	63.6% (31.6%–87.6%)	81.0% (57.4%–93.7%)
ctHHb-T-N + Ki67	25	NA	0.750	0.765	75.0% (35.6%–95.5%)	88.2% (62.3%–97.9%)	75.0% (35.6%–95.5%)	88.2% (62.3%–97.9%)
stO_2-T-N + tumor size	33	NA	0.682	0.669	72.7% (39.3%–92.7%)	77.3% (54.2%–91.3%)	61.5% (32.3%–84.9%)	85.0% (61.1%–96.0%)
Tumor size + ER	40	NA	0.827	0.866	91.7% (59.8%–99.6%)	77.3% (85.7%–66.4%)	73.3% (44.8%–91.1%)	96.0% (77.7%–99.8%)
ER + PR	40	NA	0.811	0.839	83.3% (50.9%–97.1%)	89.3% (70.6%–97.2%)	76.9% (46.0%–93.8%)	92.6% (74.2%–98.7%)

Abbreviations: LDA, linear discriminant analysis; NA, not applicable; NPV, negative predictive value; PPV, positive predictive value.

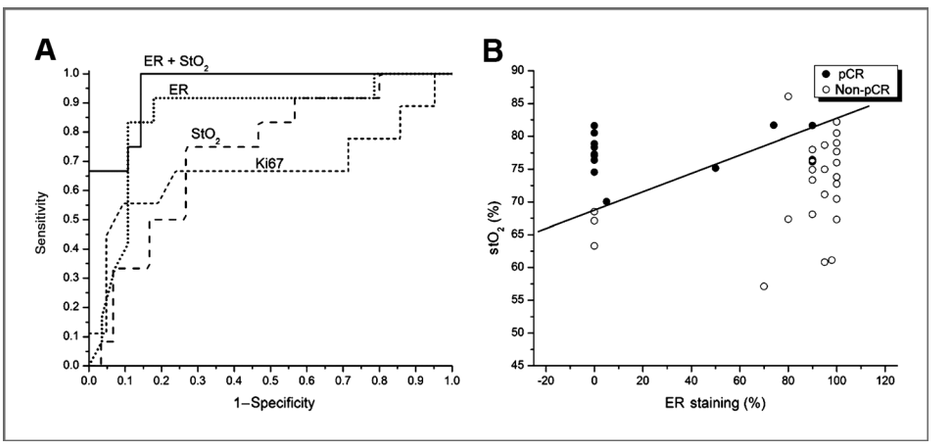

Figure 3. Results of discriminant analyses. A, ROC analysis revealed that the single feature of tumor stO_2 (AUC, 0.733) was able to discriminate pCR from non-pCR response groups with comparable accuracy to established predictive markers such as ER (AUC, 0.854) and Ki67 (AUC, 0.672). When stO_2 and ER were combined in a multivariate discriminant analysis, classification of response groups improved further (AUC, 0.955). This was the strongest combination of any parameters tested. B, the discriminator line indicates the optimal classification between pCR and non-pCR groups when stO_2 and ER were used together (sensitivity, 91.7%; specificity, 96.4%). Note that this plot visually shows the separation of pCR and non-pCR tumors using these parameters; the results reported in the text were achieved using cross-validation techniques that produced a somewhat lower discrimination accuracy.

The biologic basis for the observed associations between tumor oxygenation and chemosensitivity are potentially explained by several factors including the extent and condition of tumor vasculature, hypoxia, drug delivery, and proliferation/metabolism (40–42). Elevated levels of stO_2 could be an indication of an efficient blood supply to the tumor. This allows for better delivery of drugs and nutrients necessary to maintain replication and cell division (13, 43). In addition, in the presence of oxygen, cytotoxic drugs generate free radicals that damage DNA of cancer cells (44). Differences in stO_2 may reveal differential metabolic pathways between pCR and non-pCR tumors. Lower stO_2 in non-pCR tumors is associated with hypoxia and subsequent buildup of ctHHb. Higher stO_2 in pCR tumors reflects diminished oxygen extraction and tumor cells that are in a more proliferative state (42). This may significantly enhance chemotherapeutic efficacy, because rapidly proliferating cells are more sensitive to chemotherapy (45). Our data show that neither baseline ctO_2Hb nor ctHHb alone correlate with response and that a combination of supply and metabolism (stO_2) are necessary to explain the differences observed between pCR and non-pCR tumors.

Our observations broadly concur with the small number of other studies conducted using PET to correlate metabolic tumor properties with neoadjuvant chemotherapy response. For example, Mankoff and colleagues found that a low metabolic rate of ^{18}F-FDG relative to blood flow (measured with ^{15}O-water PET) was a predictor of complete response (27). It was hypothesized that this ratio of glucose metabolism to blood flow represents the efficiency of glucose extraction by tumors and that nonresponding, hypoxic tumors may be particularly adept at extracting glucose even in the context of poor delivery. Our observation that nonresponding tumors have lower stO_2 and relatively higher levels of ctHHb is consistent with the idea that non-pCR tumors are adept at extracting oxygen even in the presence of poor delivery. Similar trends were shown by Specht and colleagues where tumors were categorized by molecular subtypes (28).

Although this is the first published study that shows a correlation between breast cancer neoadjuvant chemotherapy response and baseline tissue oxygen saturation measurements, it is important to note that caution should be used when comparing oxygen saturation values derived using different instruments. Technical details such as the separation between the source and detector fibers, the mathematical models used for computing light propagation, whether measurements are time-dependent, time-independent, or a combination of both, and the number and selection of optical wavelengths will affect measurement accuracy and precision. More specifically, these factors will determine whether a given device is capable of adequately resolving light absorption from scattering and whether physiologic property estimates, including stO_2, are sufficiently accurate and reliable to compare different individuals. We have shown that the DOSI technology used in this study combining multifrequency, frequency-domain photon migration with spectrally broadband data has high information content and is well-suited for quantitative tissue optical and physiologic property measurements (46, 47). Interpatient comparison that uses tissue saturation devices designed for relative trending measurements may not have similar performance. Because of these challenges, methods to standardize optical tissue measurements remain an important and ongoing area of investigation.

A single handheld probe design using a fixed source–detector separation (2.8 cm) was used for all measurements in this study. It is of note that a variety of tumor sizes and depths were investigated and that relative contributions of tumor and normal tissue, also known as partial volume effects, are an inevitable consequence of this type of analysis. DOSI measurements convey a smaller fraction of the optical and functional properties of deep versus shallow tumors given equivalent

optical properties of tumor and surrounding normal tissue, tumor size, and geometry.

Despite these limitations, stO_2 measured with DOSI was a significant predictor of response. Comparable efforts have been made to assess tumor oxygenation in breast cancer using invasive microelectrodes and immunohistochemistry to derive prognostic value from determining tumor hypoxia (13, 48). Although direct measurements of tumor oxygen tension and related molecular pathways are desirable, electrodes and histochemical analyses probe highly localized tissue volumes and they require multiple insertions and fields of view, respectively, to adequately sample large tumors. These methods are susceptible to undersampling errors that can be particularly challenging in the case of microenvironmental heterogeneity. Thus, DOSI can potentially provide a noninvasive prognostic alternative by rapidly measuring global levels of tumor and normal tissue oxygenation.

In summary, this is the first study to report stO_2 as a prognostic functional optical imaging endpoint for breast cancer neoadjuvant chemotherapy before drug administration. When considered in conjunction with previous molecular imaging studies, these findings suggest a general framework for predicting individual response to chemotherapy based on the need for adequate perfusion and metabolism to support drug delivery and use, respectively. With continued standardization of the measurement and analysis technology, these features could be rapidly evaluated in the clinical oncologic workflow and may be relevant for other types of large solid tumors. Ultimately, the combination of noninvasive functional imaging endpoints and tissue-specific biomarkers may provide a promising strategy for predicting individual patient chemotherapy responsiveness and guiding clinical decision-making. This information could be used, for example, in subjects who are likely to be nonresponders where neoadjuvant chemotherapy would offer no benefit and subjects might endure significant side effects. These individuals could immediately undergo surgical resection with no change in overall outcome. DOSI may also have use in devising new treatment strategies by providing oncologists with feedback on drugs that enhance tumor perfusion before the administration of cytotoxic agents.

Disclosure of Potential Conflicts of Interest

A. Cerussi and B.J. Tromberg report patents, which are owned by the University of California, that are related to the technology and analysis methods described in this study. The University of California has licensed diffuse optical spectroscopic imaging technology and analysis methods to two companies, FirstScan, Inc. and Volighten, Inc., for different fields of use, including breast cancer (FirstScan, Inc.). This research was completed without participation, knowledge, or financial support of either company, and data were acquired and processed from patients by coauthors unaffiliated with either entity. The Institutional Review Board and Conflict of Interest Office of the University of California, Irvine, have reviewed both patent and corporate disclosures and did not find any concerns. No potential conflicts of interest were disclosed by the other authors.

Authors' Contributions

Conception and design: S. Ueda, D. Roblyer, A. Cerussi, D. Hsiang, R. Mehta, B.J. Tromberg

Development of methodology: S. Ueda, D. Roblyer, A. Cerussi, D. Hsiang, R. Mehta, B.J. Tromberg

Acquisition of data (provided animals, acquired and managed patients, provided facilities, etc.): S. Ueda, A. Durkin, A. Leproux, Y. Santoro, S. Xu, D. Hsiang, R. Mehta, J. Butler

Analysis and interpretation of data (e.g., statistical analysis, biostatistics, computational analysis): S. Ueda, D. Roblyer, S. Xu, T.D. O'Sullivan, D. Hsiang

Writing, review, and/or revision of the manuscript: S. Ueda, D. Roblyer, A. Cerussi, S. Xu, D. Hsiang, R. Mehta, J. Butler, B.J. Tromberg

Administrative, technical, or material support (i.e., reporting or organizing data, constructing databases): D. Roblyer, A. Durkin, D. Hsiang, R. Mehta

Study supervision: A. Cerussi, R. Mehta, B.J. Tromberg

Acknowledgments

The authors thank Montana Compton for her assistance and the patients who generously volunteered their time for this study and Christine McLaren and Wen-Pin Chen for their assistance with statistical analysis.

Grant Support

This work was supported by the NIH under grants P41-EB015890 (Laser Microbeam and Medical Program: LAMMP), U54-CA136400, R01-CA142989, P30-CA62203 (University of California, Irvine Cancer Center Support Grant), and the American College of Radiology Imaging Networks (ACRIN). D. Roblyer acknowledges support from the DOD Era of Hope Fellowship Program (W81XWH-10-1-0972). D. Roblyer and T.D. O'Sullivan acknowledge support from the UCI Cancer Research Institute Training grant (NCI-T32CA009054). BLI programmatic support from the Beckman Foundation is acknowledged. The diffuse optical spectroscopic imaging instrumentation used in this study was constructed in a university laboratory using federal grant support (NIH).

The costs of publication of this article were defrayed in part by the payment of page charges. This article must therefore be hereby marked *advertisement* in accordance with 18 U.S.C. Section 1734 solely to indicate this fact.

Received January 6, 2012; revised June 1, 2012; accepted June 19, 2012; published OnlineFirst July 9, 2012.

References

1. Smith IC, Heys SD, Hutcheon AW, Miller ID, Payne S, Gilbert FJ, et al. Neoadjuvant chemotherapy in breast cancer: significantly enhanced response with docetaxel. J Clin Oncol 2002;20:1456–66.
2. Kaufmann M, von Minckwitz G, Bear HD, Buzdar A, McGale P, Bonnefoi H, et al. Recommendations from an international expert panel on the use of neoadjuvant (primary) systemic treatment of operable breast cancer: new perspectives 2006. Ann Oncol 2007;18:1927–34.
3. Fisher B, Bryant J, Wolmark N, Mamounas E, Brown A, Fisher ER, et al. Effect of preoperative chemotherapy on the outcome of women with operable breast cancer. J Clin Oncol 1998;16:2672–85.
4. Sachelarie I, Grossbard ML, Chadha M, Feldman S, Ghesani M, Blum RH. Primary systemic therapy of breast cancer. Oncologist 2006;11:574–89.
5. Rastogi P, Anderson SJ, Bear HD, Geyer CE, Kahlenberg MS, Robidoux A, et al. Preoperative chemotherapy: updates of National Surgical Adjuvant Breast and Bowel Project Protocols B-18 and B-27. J Clin Oncol 2008;26:778–85.
6. Guarneri V, Broglio K, Kau SW, Cristofanilli M, Buzdar AU, Valero V, et al. Prognostic value of pathologic complete response after primary chemotherapy in relation to hormone receptor status and other factors. J Clin Oncol 2006;24:1037–44.
7. Andre F, Broglio K, Roche H, Martin M, Mackey JR, Penault-Llorca F, et al. Estrogen receptor expression and efficacy of docetaxel-containing adjuvant chemotherapy in patients with node-positive breast cancer: results from a pooled analysis. J Clin Oncol 2008;26:2636–43.
8. Sanchez-Munoz A, Garcia-Tapiador AM, Martinez-Ortega E, Duenas-Garcia R, Jaen-Morago A, Ortega-Granados AL, et al. Tumour molecular subtyping according to hormone receptors and HER2 status defines different pathological complete response to neoadjuvant chemotherapy in patients with locally advanced breast cancer. Clin Transl Oncol 2008;10:646–53.
9. Harris L, Fritsche H, Mennel R, Norton L, Ravdin P, Taube S, et al. American Society of Clinical Oncology 2007 update of recommenda-

tions for the use of tumor markers in breast cancer. J Clin Oncol 2007; 25:5287–312.
10. Bevilacqua F, Berger AJ, Cerussi AE, Jakubowski D, Tromberg BJ. Broadband absorption spectroscopy in turbid media by combined frequency-domain and steady-state methods. Appl Opt 2000;39: 6498–507.
11. Pakalniskis MG, Wells WA, Schwab MC, Froehlich HM, Jiang S, Li Z, et al. Tumor angiogenesis change estimated by using diffuse optical spectroscopic tomography: demonstrated correlation in women undergoing neoadjuvant chemotherapy for invasive breast cancer? Radiology 2011;259:365–74.
12. Denko NC. Hypoxia, HIF1 and glucose metabolism in the solid tumour. Nat Rev Cancer 2008;8:705–13.
13. Vaupel P, Schlenger K, Knoop C, Hockel M. Oxygenation of human tumors: evaluation of tissue oxygen distribution in breast cancers by computerized O2 tension measurements. Cancer Res 1991;51: 3316–22.
14. Okunieff P, Hoeckel M, Dunphy EP, Schlenger K, Knoop C, Vaupel P. Oxygen tension distributions are sufficient to explain the local response of human breast tumors treated with radiation alone. Int J Radiat Oncol Biol Phys 1993;26:631–6.
15. Finlay JC, Foster TH. Hemoglobin oxygen saturations in phantoms and *in vivo* from measurements of steady-state diffuse reflectance at a single, short source-detector separation. Med Phys 2004;31: 1949–59.
16. Finlay JC, Foster TH. Recovery of hemoglobin oxygen saturation and intrinsic fluorescence with a forward-adjoint model. Appl Opt 2005;44: 1917–33.
17. Wang HW, Zhu TC, Putt ME, Solonenko M, Metz J, Dimofte A, et al. Broadband reflectance measurements of light penetration, blood oxygenation, hemoglobin concentration, and drug concentration in human intraperitoneal tissues before and after photodynamic therapy. J Biomed Opt 2005;10:14004.
18. Cerussi A, Shah N, Hsiang D, Durkin A, Butler J, Tromberg BJ. *In vivo* absorption, scattering, and physiologic properties of 58 malignant breast tumors determined by broadband diffuse optical spectroscopy. J Biomed Opt 2006;11:044005.
19. Cerussi A, Hsiang D, Shah N, Mehta R, Durkin A, Butler J, et al. Predicting response to breast cancer neoadjuvant chemotherapy using diffuse optical spectroscopy. Proc Natl Acad Sci U S A 2007;104: 4014–9.
20. Soliman H, Gunasekara A, Rycroft M, Zubovits J, Dent R, Spayne J, et al. Functional imaging using diffuse optical spectroscopy of neoadjuvant chemotherapy response in women with locally advanced breast cancer. Clin Cancer Res 2010;16:2605–14.
21. Zhu Q, Tannenbaum S, Hegde P, Kane M, Xu C, Kurtzman SH. Noninvasive monitoring of breast cancer during neoadjuvant chemotherapy using optical tomography with ultrasound localization. Neoplasia 2008;10:1028–40.
22. Jiang S, Pogue BW, Carpenter CM, Poplack SP, Wells WA, Kogel CA, et al. Evaluation of breast tumor response to neoadjuvant chemotherapy with tomographic diffuse optical spectroscopy: case studies of tumor region-of-interest changes. Radiology 2009;252: 551–60.
23. Esserman L, Kaplan E, Partridge S, Tripathy D, Rugo H, Park J, et al. MRI phenotype is associated with response to doxorubicin and cyclophosphamide neoadjuvant chemotherapy in stage III breast cancer. Ann Surg Oncol 2001;8:549–59.
24. Uematsu T, Kasami M, Yuen S. Neoadjuvant chemotherapy for breast cancer: correlation between the baseline MR imaging findings and responses to therapy. Eur Radiol 2010;20:2315–22.
25. Li XR, Cheng LQ, Liu M, Zhang YJ, Wang JD, Zhang AL, et al. DW-MRI ADC values can predict treatment response in patients with locally advanced breast cancer undergoing neoadjuvant chemotherapy. Med Oncol 2012;29:425–31.
26. Nilsen L, Fangberget A, Geier O, Olsen DR, Seierstad T. Diffusion-weighted magnetic resonance imaging for pretreatment prediction and monitoring of treatment response of patients with locally advanced breast cancer undergoing neoadjuvant chemotherapy. Acta Oncol 2010;49:354–60.
27. Mankoff DA, Dunnwald LK, Gralow JR, Ellis GK, Schubert EK, Tseng J, et al. Changes in blood flow and metabolism in locally advanced breast cancer treated with neoadjuvant chemotherapy. J Nucl Med 2003;44: 1806–14.
28. Specht JM, Kurland BF, Montgomery SK, Dunnwald LK, Doot RK, Gralow JR, et al. Tumor metabolism and blood flow as assessed by positron emission tomography varies by tumor subtype in locally advanced breast cancer. Clin Cancer Res 2010;16:2803–10.
29. Cerussi A, Siavoshi S, Durkin A, Chen C, Tanamai W, Hsiang D, et al. Effect of contact force on breast tissue optical property measurements using a broadband diffuse optical spectroscopy handheld probe. Appl Opt 2009;48:4270–7.
30. Acrin 6691 Training Videos. 2012. [cited Jan 6, 2012]. Available from: http://acrin.bli.uci.edu/trainingvideos.
31. Roblyer D, Ueda S, Cerussi A, Tanamai W, Durkin A, Mehta R, et al. Optical imaging of breast cancer oxyhemoglobin flare correlates with neoadjuvant chemotherapy response one day after starting treatment. Proc Natl Acad Sci U S A 2011;108:14626–31.
32. Tromberg BJ, Cerussi A, Shah N, Compton M, Durkin A, Hsiang D, et al. Imaging in breast cancer: diffuse optics in breast cancer: detecting tumors in pre-menopausal women and monitoring neoadjuvant chemotherapy. Breast Cancer Res 2005;7:279–85.
33. Bloom HJ, Richardson WW. Histological grading and prognosis in breast cancer; a study of 1409 cases of which 359 have been followed for 15 years. Br J Cancer 1957;11:359–77.
34. Vergara IA, Norambuena T, Ferrada E, Slater AW, Melo F. StAR: a simple tool for the statistical comparison of ROC curves. BMC Bioinformatics 2008;9:265.
35. Tan MC, Al Mushawah F, Gao F, Aft RL, Gillanders WE, Eberlein TJ, et al. Predictors of complete pathological response after neoadjuvant systemic therapy for breast cancer. Am J Surg 2009;198:520–5.
36. Jones RL, Salter J, A'Hern R, Nerurkar A, Parton M, Reis-Filho JS, et al. Relationship between oestrogen receptor status and proliferation in predicting response and long-term outcome to neoadjuvant chemotherapy for breast cancer. Breast Cancer Res Treat 2010;119:315–23.
37. Colleoni M, Viale G, Goldhirsch A. Lessons on responsiveness to adjuvant systemic therapies learned from the neoadjuvant setting. Breast 2009;18 Suppl 3:S137–40.
38. Kuerer HM, Newman LA, Smith TL, Ames FC, Hunt KK, Dhingra K, et al. Clinical course of breast cancer patients with complete pathologic primary tumor and axillary lymph node response to doxorubicin-based neoadjuvant chemotherapy. J Clin Oncol 1999;17:460–9.
39. Straver ME, Rutgers EJ, Rodenhuis S, Linn SC, Loo CE, Wesseling J, et al. The relevance of breast cancer subtypes in the outcome of neoadjuvant chemotherapy. Ann Surg Oncol 2010;17:2411–8.
40. Warburg O. On respiratory impairment in cancer cells. Science 1956;124:269–70.
41. Racker E. Warburg effect revisited. Science 1981;213:1313.
42. Vander Heiden MG, Cantley LC, Thompson CB. Understanding the Warburg effect: the metabolic requirements of cell proliferation. Science 2009;324:1029–33.
43. Vaupel P, Thews O, Kelleher DK, Hoeckel M. Oxygenation of human tumors: the Mainz experience. Strahlenther Onkol 1998;174 Suppl 4: 6–12.
44. Tredan O, Galmarini CM, Patel K, Tannock IF. Drug resistance and the solid tumor microenvironment. J Natl Cancer Inst 2007;99:1441–54.
45. Huang LE, Bindra RS, Glazer PM, Harris AL. Hypoxia-induced genetic instability–a calculated mechanism underlying tumor progression. J Mol Med 2007;85:139–48.
46. Fujimoto JG, Farkas DL, editors. Biomedical optical imaging. New York, NY: Oxford University Press; 2009.
47. Boas DA, Pitris C, Ramanujam N, editors. Handbook of biomedical optics. Boca Raton, FL: CRC Press; 2011.
48. Hohenberger P, Felgner C, Haensch W, Schlag PM. Tumor oxygenation correlates with molecular growth determinants in breast cancer. Breast Cancer Res Treat 1998;48:97–106.